



Optimizing the Power Performance of Lithium-Ion Batteries: The Role of Separator Porosity and Electrode Mass Loading

Seungyeop Choi^{+, [a]} Jun Pyo Seo^{+, [a]} Jaejin Lim^{+, [a]} Cyril Bubu Dzakpasu,^[b] Youngjoon Roh,^[b] Cheol Bak,^[b] Suhwan Kim,^[b] Hongkyung Lee,^{*[c, d]} and Yong Min Lee^{*[a, b, d]}

This study investigates the concealed effect of separator porosity on the electrochemical performance of lithium-ion batteries (LIBs) in thin and thick electrode configuration. The effect of the separator is expected to be more pronounced in cells with thin electrodes due to its high volumetric/resistance ratio within the cell. However, the electrochemical analyses show similar power performance regardless of the separator porosity in the thin electrode configuration. In contrast, for cells with thick electrodes, separator porosity significantly impacts the direct current-internal resistance (DC-IR) and the capacity retention at a high rate. This behavior is attributed to ion

concentration gradients in the upper regions of thick electrodes, while Li⁺ transfer to lower regions is hampered as the electrode thickness increases. These findings suggest that the intrinsic properties of individual cell components, such as separator porosity, are highly dependent on the overall cell design. Moreover, while high-porosity separators enhance power performance, particularly in thick electrode configurations, they exhibit lower thermal stability and tensile strength. In conclusion, this study highlights the need for an integrated approach to optimizing separator characteristics, considering both electrochemical performance and safety trade-offs in LIBs.

Introduction

The application of lithium-ion batteries (LIBs) has expanded from small electronic gadgets to large-format energy storage systems, including electric vehicles, drones, and military equipment.^[1–4] Consequently, depending on the application, LIBs demand specific characteristics such as high-power performance, high energy density, and safety. Much research initially focused on the development of electrode and electrolyte materials to meet these requirements.^[5–13] In recent times, the focus has also been on improving the electrochemical performance of LIBs by optimizing the cell design. One notable approach to enhancing power performance involves using thin

electrodes due to their low internal resistance and short ion transport distances. Conversely, thick electrodes can reduce the volumetric ratio of inactive materials such as separator, current collector or lead tabs to active materials, thereby resulting in LIBs with higher energy density. However, the long and high tortuous ion transport distances can compromise the power capability.^[14–21]

Along with optimizing cell design through electrode loading, various other inactive components have also been considered. Among them, the effect of the internal microstructure and additional ceramic coating layer of the separator on the electrochemical performance of LIBs has already been investigated.^[22–30] Especially, the thickness of the separator is a key design parameter affecting the impedance and ionic conductivity. By reducing the thickness of the base separator film or the ceramic coating layer, the resistance of the separator can be lowered, which can enhance the power performance and energy density of the LIBs.^[31–33] However, even with the same thickness of separators, significant differences in physical and electrochemical properties have been observed depending on their pore structure.^[34] Typically, since separators with lower porosity can have a smaller amount of liquid electrolyte within more tortuous pore structures, good power capability cannot be achieved.

In this context, R.E. Sousa et al.^[35] reported that PVdF-HFP separators with high porosity exhibit excellent ionic conductivity and electrolyte wettability compared to the low porosity PVdF-HFP counterparts, thus inducing superior discharge capacity in high C-rate. Similarly, Y. Lee et al.^[36] systematically investigated the effect of the pore structure of polyethylene (PE) separators on the electrochemical performance of LIBs. They noted that the ionic conductance of the separators, which

[a] S. Choi,⁺ J. P. Seo,⁺ J. Lim,⁺ Prof. Y. M. Lee

Department of Chemical and Biomolecular Engineering

Yonsei University

50 Yonsei-ro, Seodaemun-gu, Seoul 03722, Republic of Korea

E-mail: yongmin@yonsei.ac.kr

[b] C. B. Dzakpasu, Y. Roh, C. Bak, S. Kim, Prof. Y. M. Lee

Department of Energy Science and Engineering

Daegu Gyeongbuk Institute of Science and Technology (DGIST)

Daegu 42988, Republic of Korea

[c] Prof. H. Lee

Department of Materials Science and Engineering

Yonsei University

50 Yonsei-ro, Seodaemun-gu, Seoul 03722, Republic of Korea

E-mail: hongkyung.lee@yonsei.ac.kr

[d] Prof. H. Lee, Prof. Y. M. Lee

Department of Battery Engineering

Yonsei University

50 Yonsei-ro, Seodaemun-gu, Seoul 03722, Republic of Korea

[+] These authors contributed equally to this work

Supporting information for this article is available on the WWW under <https://doi.org/10.1002/batt.202400638>

is commonly proportional to their porosity, is closely related to the rate capabilities. Likewise, the effect of separator porosity on the electrochemical performance of LIBs has been conducted by a few research groups. However, most of them did not seriously consider the influence of electrode design factors such as loading level, which greatly governs the overall electrochemical performances of LIBs. To adopt an ideal separator, it is important to understand the effect of the separator on the electrochemical performance of LIBs with different electrode designs. In addition, because high porosity separators usually have low thermal stability and mechanical strength, it is important to select an appropriate separator for each electrode design.^[37–39]

Thus, in this study, we attempt to correlate the effect of the porosity of the separator on the electrochemical performance with different electrode pairs: one with a high loading level (HL) and the other with a low loading level (LL) while maintaining an N/P ratio of 1.13. Also, two kinds of PE separators, with a high porosity (HP) of 58.2% and low porosity (LP) of 37.2% samples but with the same thickness of 9 µm, were chosen to assemble four different LIB cell configurations, LL-HP, LL-LP, HL-HP, and HL-LP. First, we analyzed physical properties like Gurley number and ionic conductivity of each separator. In addition, the rate capability, cycle performance at low and high C-rates, direct current-internal resistance (DC-IR), etc., of the four LIB cells were compared to understand how the separator's porosity influences the electrochemical characteristics of LIBs. Also, we developed an electrochemical model to analyze the influence of the separator on the electrochemical performance of various electrode types under high-power operating conditions. Furthermore, the thermal stability and mechanical properties of each separator with different porosities were investigated to explore a correlation between safety and power performance. Thus, this work will serve as a helpful manual for understanding the effects of separator porosity on the electrochemical performance and safety of LIBs with thick/thin electrodes.

Results and Discussion

We prepared two types of cathodes, one with a high loading level (HL) of 23.5 mg cm^{-2} and the other with a low loading level (LL) of 9.4 mg cm^{-2} , as well as the corresponding anodes with an N/P ratio of 1.13, as detailed in the Experimental section. Additionally, we prepared two 9 µm-thick PE separators with different porosities. The high porosity (HP) PE separator had a porosity of 58.2%, while the low porosity (LP) PE separator had a porosity of 37.2%. Using each cathode with the respective anode, we fabricated four different cell configurations (LL-HP, LL-LP, HL-HP, and HL-LP) using the HP and LP separators, as schematically illustrated in Figure 1.

The ionic and electronic resistance of the electrodes for each configuration are presented in Figure 2. The ionic resistance (R_{ion}) represents the resistance encountered by Li^+ ions as they move through the electrolyte within the pores in the composite electrodes. From symmetric cell electrochemical impedance spectroscopy (EIS) and the corresponding equiva-

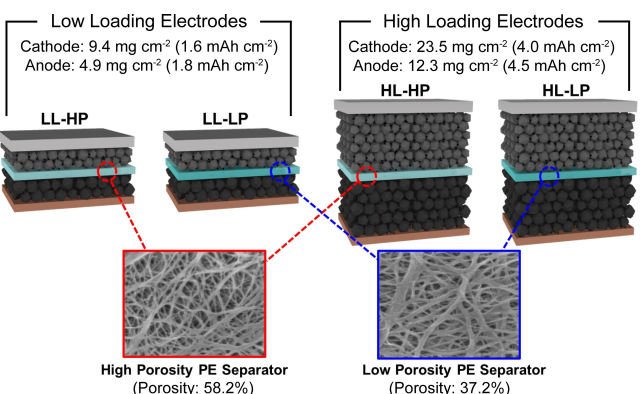


Figure 1. Schematic images of the four different cell configurations: low loading level electrode-high porosity PE separator (LL-HP), low loading level electrode-low porosity PE separator (LL-LP), high loading level electrode-high porosity PE separator (HL-HP), and high loading level electrode-low porosity PE separator (HL-LP).

lent circuit model, the R_{ion} of the electrode can be estimated (Figures 2a and b).^[40–43] An evident change in R_{ion} was observed depending on the electrode loading level (e.g., the HL cathode exhibited an R_{ion} value approximately 180% higher than that of the LL cathode) (Figures 2c and d). However, bulk electronic resistivities of the HL and LL electrodes did not show significant differences (Figures 2e and f). This observation can be attributed to the use of the same components, compositions, and densities in fabricating the electrodes despite the variations in loading level. Additionally, as shown in Figure S1, no morphological differences were observed between the HL and LL electrodes. However, the resistance of the electrode/current collector interface was more than twice as high for the HL electrodes compared to the LL electrodes, because the electronic conduction network in the thickness direction becomes less uniform as the electrode becomes thicker (Figure 2g and h).^[44,45] Based on these results, we can infer that the HL electrodes may introduce significant resistance within the cell compared to the LL electrodes.

In addition to the resistance properties of the electrodes, the physical properties of the separators used in this study are summarized in Table 1. Even though the HP and LP separators have the same thickness, they exhibit differences in their internal microstructures, which can also be observed in the surface SEM images of each separator (Figure S2). The LP separator contains more fibers, resulting in a higher weight per unit area (gram per square meter, GSM) and a concurrently higher Gurley number ($63.6 \text{ s } 100 \text{ mL}^{-1}$ for the HP separator and $159.5 \text{ s } 100 \text{ mL}^{-1}$ for the LP separator). These microstructural differences also contributed to increased resistance within the separators, with the LP separator demonstrating approximately a 40% higher resistance than the HP separator, leading to a substantial difference in ionic conductivity (see Figure S3 for the AC impedance spectra of stainless steel (SUS)/separator/SUS cells with the HP and LP separators). Notably, since both separators are made of the same PE material, they exhibit the same contact angle, as evident from Figure S4. This highlights

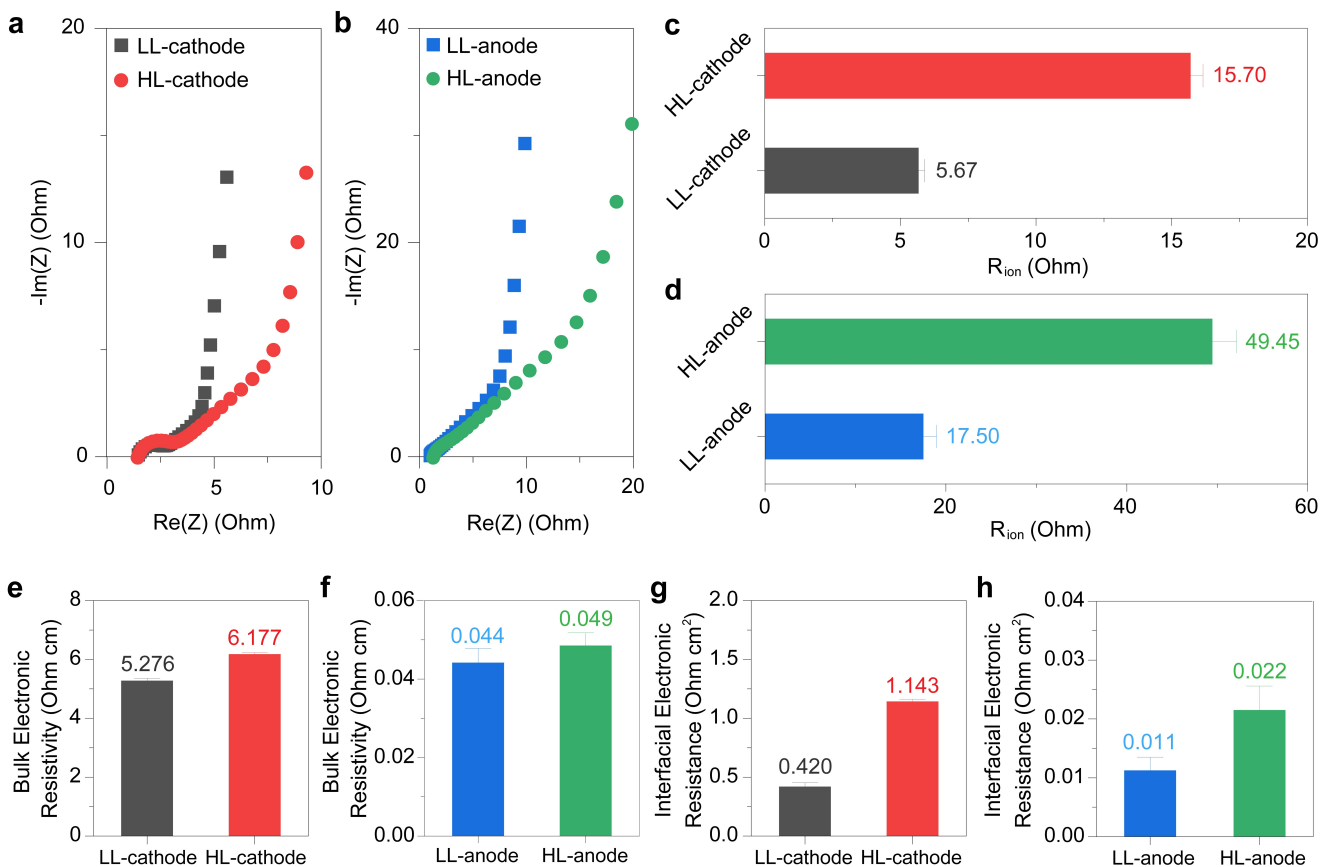


Figure 2. Symmetric cell electrochemical impedance spectra (EIS) of the (a) LL and HL cathodes and (b) LL and HL anodes. Ionic resistance plots estimated from the symmetric cell EIS of the (c) LL and HL cathodes and (d) LL and HL anodes. Bulk resistivity of (e) cathodes, (f) anodes, and interfacial resistance of (g) cathodes, (h) anodes at the electrode/current collector interface.

that the difference in ionic conductivity is due to the internal microstructure of the separators.

Furthermore, when we sum up the resistance due to the electrode design and the resistance within the separators, it is expected that the HL-LP cell will have the highest resistance among the four different cell configurations, followed by HL-HP, LL-LP, and LL-HP cells. Specifically, in both cases where HL and LL electrodes are used, the different resistance of the HP and LP separators can affect the power performance of the LIBs. However, apart from the resistance differences of each electrode, considering that the difference in the volumetric or resistance ratio of the separator between the HL and LL cells (the HL cell has a lower volumetric/resistance ratio of the separator)—it can be inferred that the power performance of the

LL cell is more significantly affected by the porosity of the separator.^[19] However, this represents only the resistance between each component and does not encompass the resistance of the overall cell system. Thus, to analyze the actual resistance and differences in electrochemical performance in real cells, we conducted electrochemical tests, as shown in Figure 3. From the initial charge-discharge voltage curves of each cell in Figure S5, it is evident that there is no significant difference in initial charge/discharge capacities and Coulombic efficiencies. Additionally, from the low C-rate (0.5 C) cycle performance as shown in Figure 3a, there are no notable differences in capacity retention and Coulombic efficiencies among the four cells. However, from the high C-rate (3 C) cycle performance in Figure 3b, the HL and LL cells exhibit significant

Table 1. Physical and ion-conductive properties of the high porosity (HP) and low porosity (LP) PE separators.

Separator	Thickness (μm)	GSM ^[a]	Gurley Number ($\text{s } 100\text{ mL}^{-1}$)	Resistance (Ohm)	Ionic Conductance (S)	Ionic Conductivity (mS cm^{-1})
HP separator	9	3.54	63.6	0.508	1.968	0.881
LP separator	9	5.31	159.5	0.897	1.114	0.499

[a] Gram per Square Meter.

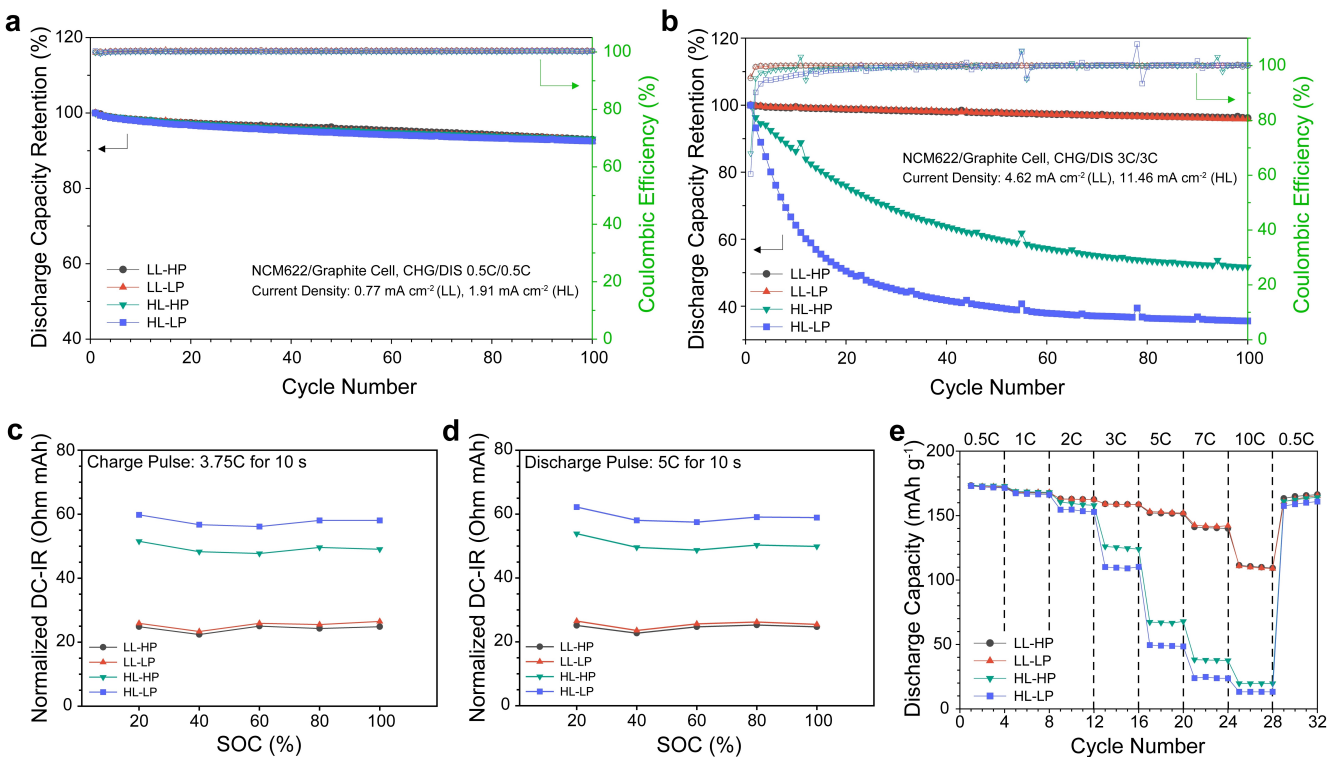


Figure 3. Cycle performances at (a) 0.5 C-rate and (b) 3 C-rate of the four cells (LL-HP, LL-LP, HL-HP, and HL-LP). (c) 10 s charge and (d) 10 s discharge DC-IRs of the four cells (LL-HP, LL-LP, HL-HP, and HL-LP). (e) Rate capabilities of the four cells as a function of the discharging C-rate (0.5 C, 1 C, 2 C, 3 C, 5 C, 7 C, 10 C, and 0.5 C) while maintaining the same charging C-rate of 0.5 C.

differences in discharge capacity retention. The high-resistance HL cells experience a substantial decrease in capacity retention as cycling progresses, dropping below 60% capacity retention after 100 cycles. Particularly, the HL-LP cell, with even higher resistance, exhibits a more pronounced decline, reaching below approximately 50% capacity retention only after 20 cycles. In contrast, the low-resistance LL cells demonstrate excellent capacity retention even after 100 cycles, and similar behavior in capacity retention is observed regardless of the porosity of the separators. Thus, despite the LL cells having a higher volumetric/resistance proportion of the separator, there are no differences in cycle performance, even at high C-rates. This indicates that power performance is not simply proportional to the sum of the resistances of each component, especially in the LL cells.

To comprehensively measure the overall resistance of each cell system, we conducted state-of-charge (SOC)-dependent DC-IR measurements using hybrid pulse power characterization (HPPC) evaluations. To normalize the DC-IR value, we multiplied the DC-IR values by the capacity (mAh) of the HL and LL cells, enabling a comparison between cells with different electrode loading levels.^[46] As shown in Figures 3c and d, the DC-IRs were consistently higher for the HL cells during both charge and discharge. Especially consistent with the previous results in Figure 3b, the LL cells exhibited less resistance variation due to the separator. In contrast, the HL cells showed a more significant difference depending on the separator type (see Figure S6 for the time-voltage curves at a SOC of 20% of each cell). Moreover, from the rate capabilities of the four cells, as

shown in Figure 3e, the LL cells (LL-HP and LL-LP) did not show significant differences in capacity retention as a function of the porosity of the separator, even at a very high C-rate of 10 C. However, for the HL cells (HL-HP and HL-LP), a difference in capacity retention due to separator porosity was observed above 2 C-rate. Based on these results, we can strongly conclude that the ion-conductive properties of the separator may or may not manifest, depending on the overall cell design.

To unravel the different effects of separators on the power performance in the HL and LL cells, we developed an electrochemical model for simulating the 3 C-rate fast discharging process. Specifically, we built a pseudo-3-dimensional (P3D) $\text{LiNi}_{0.6}\text{Co}_{0.2}\text{Mn}_{0.2}\text{O}_2$ NCM622/graphite full cell model incorporating the actual separator geometry and electrochemical properties, achieving a discharge capacity highly consistent with the experimental results shown in Figure 3e (Figure 4a). As the HP and LP separators possess nearly a two-times difference in ionic conductivity (Table 1) and given that the separator serves as a Li^+ channel between the cathode and anode, we hypothesized that the Li^+ concentration in the electrolyte would vary depending on the separator properties. The simulation results in Figure 4b show that, while the average Li^+ concentration in the electrolyte did not exhibit a significant change depending on the separators in the LL-cathode, a clear difference was observed in the HL-cathode. To further analyze the distribution of Li^+ concentration in the electrolyte for the HL cathode, we visualized the Li^+ concentration distribution in the electrolyte as a function of discharge capacity and normalized electrode

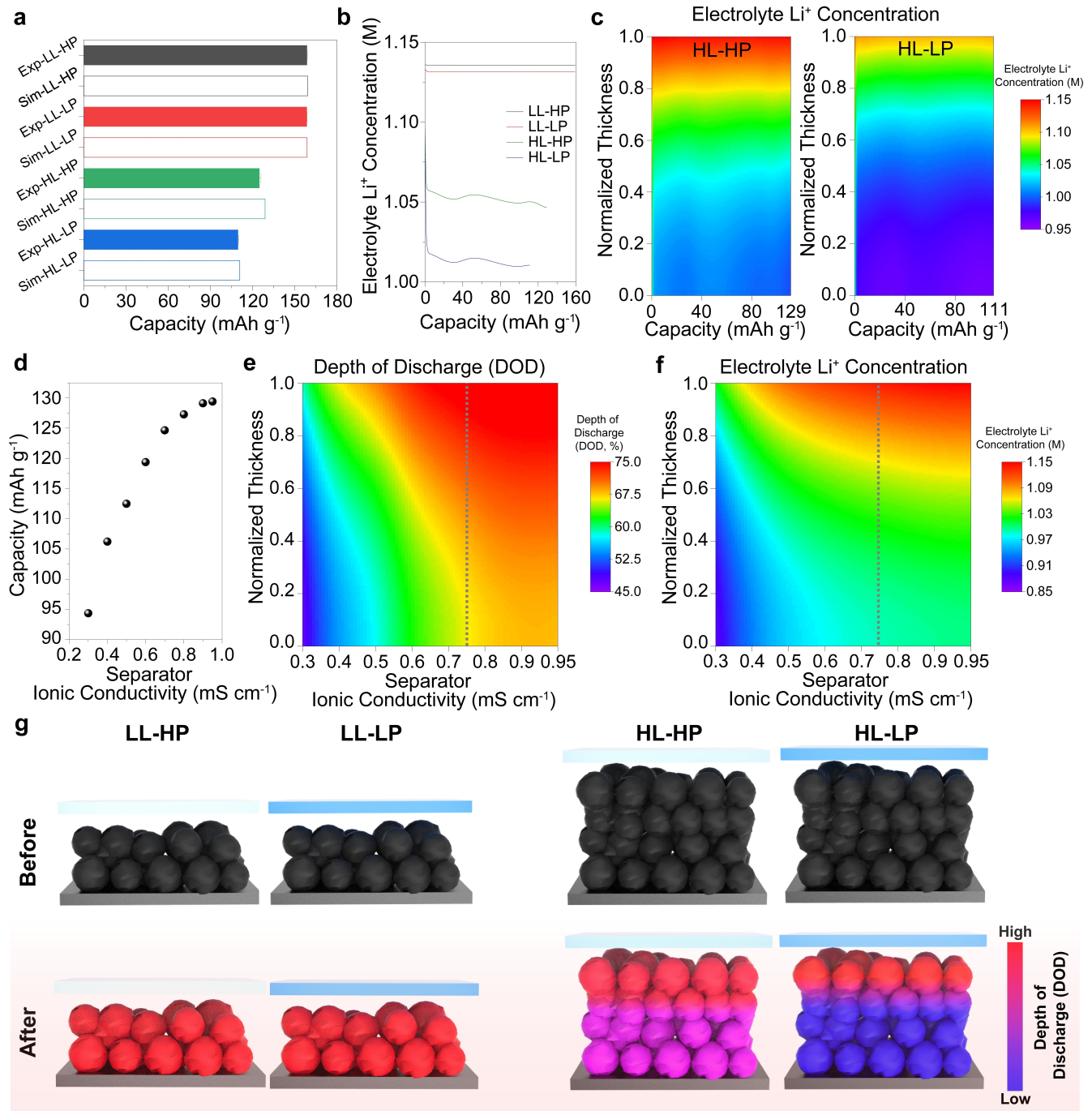


Figure 4. 3 C-rate fast discharge simulation results. (a) Comparison of discharge capacities between experiment and simulation. (b) Average electrolyte Li^+ concentration for the four cells (LL-HP, LL-LP, HL-HP, and HL-LP). (c) Electrolyte Li^+ concentration of the cathode as a function of the discharge capacity and normalized thickness in the HL configuration. (d) Discharge capacity, (e) depth of discharge, and (f) electrolyte Li^+ concentration with varying separator ionic conductivities at the end of discharge. (g) Schematic illustration of the separator's effect on the power performance with different cell configurations.

thickness (current collector; 0.0 and electrode surface; 1.0) in Figures 4c and S7. The HL-HP configuration showed a higher electrolyte ion concentration at the upper region of the electrode compared to the HL-LP, implying that the ionic-conductive properties of the separator can significantly influence the electrolyte ion concentration within composite electrodes under high-power operation conditions. During the 3 C-rate discharge process, Li^+ is delithiated from the anode

and diffuse/migrate through the separator to the cathode. Thus, a separator with low ionic conductivity can hinder the supply of Li^+ to the cathode. Moreover, this hindrance becomes more severe as the Li^+ flux, current density, or loading level increases. Also, any interference in the Li^+ supply through the separator decreases the Li^+ concentration within the cathode electrolyte. Additionally, increased electrode thickness and R_{ion} due to a higher loading level can impede Li^+ transfer from the

upper to the lower region of the electrode, leading to a substantial concentration gradient of Li^+ . Therefore, in HL cells, the reduction in Li^+ supply to the upper part of the electrode due to increased separator resistance, along with the concentration gradient occurring within the electrode, can lead to a significant reduction in capacity. The simulation results in Figures 4c and S7 strongly support this hypothesis, showing a pronounced Li^+ concentration gradient between the upper and lower regions of the HL cathode. In contrast, no significant difference and gradient in the Li^+ concentration was observed within the electrode for the LL configuration. Therefore, the resistance difference in the separator amplifies the variation in the electrochemical performance of the electrode in the HL configuration, which is not significant in the LL configuration. Based on this observation, to investigate the minimum ionic conductivity required for the separator to achieve sufficient power performance in the HL cell, we performed 3 C-rate discharge simulations while varying the separator ionic conductivity from 0.3 to 0.95 mS cm^{-1} (0.3, 0.4, 0.5, 0.6, 0.7, 0.8, 0.9, and 0.95 mS cm^{-1}). The discharge capacity increased with increasing ionic conductivity, however particularly beyond 0.8 mS cm^{-1} , it saturated (Figure 4d). To analyze this result, we examined the depth of discharge (DOD) of the cathode and the distribution of electrolyte Li^+ concentration at the end of the discharge as a function of separator ionic conductivity (Figures 4e and f). As shown in Figure 4e, the DOD increased with increasing ionic conductivities, and the electrolyte Li^+ concentration shows similar behavior (Figure 4f). However, it was confirmed that the DOD and electrolyte Li^+ concentration distribution converged at ionic conductivities above approximately 0.75 mS cm^{-1} (gray line in Figures 4e and f). Therefore, in HL configurations, the ionic conductivity of the separator must reach a certain threshold value to ensure sufficient power performance. For the HL configuration examined in this study, this threshold value was determined to be 0.75 mS cm^{-1} . In summary, as schematically illustrated in Figure 4g, the ionic conductivity of the separator manifests its effect depending on the specific electrode configuration, and the influence on power performance is maximized as the electrode loading level increases.

Finally, even though the HP separator exhibits favorable electrochemical performance in both the HL and LL cells, we cannot overlook safety considerations in cell design. As shown in the thermal shrinkage test in Figure 5a, the HP separator exhibits higher thermal shrinkage than the LP separator at high temperatures (120, 130, and 140°C for 30 min). In addition, as shown in Figure S8, after exposure to 130°C for 30 min, pore blocking was observed in the HP separator, while the LP separator maintained its pore structure quite well. To confirm how the thermal stability of separators impacts the safety of actual cells, pouch-type NCM622/graphite cells were fabricated using the HP and LP separators (Figure S9). Each cell was fully charged to 4.3 V and then exposed to 140°C while measuring the open-circuit voltage (OCV) over time (Figure 5b). Consistent with the thermal shrinkage test, the pouch cell with the LP separator survived longer than the HP separator cell (20.0 min for HP separator and 39.5 min for LP separator). Thus, although

using the HP separator in HL cells may provide better power performance, it could potentially compromise the safety of the cell. On the other hand, in the case of LL cells, since the porosity of the separator does not significantly affect power performance (Figures 3 and 4), using the LP separator is highly recommended for high-safety LIBs. Furthermore, along with the thermal shrinkage test, we also measured the tensile strength of each separator, which is also crucial for high-safety LIBs as it helps maintain mechanical stability during cell manufacturing and operation. As shown in Figure 5c, the LP separator showed higher tensile strength than the HP separator (124.4 and 152.6 MPa for the HP and LP separators, respectively). Thus, it is essential to select ideal separators considering the balance between safety and power performance, especially in the HL cell configuration.

Conclusions

In summary, we investigated the influence of high- and low-porosity separators on power performance, depending on the loading levels of the cathode and anode (thick or thin electrodes). By thoroughly analyzing the resistance contributions from both the electrodes and separators, we initially hypothesized that the effect of separator resistance would be more pronounced in cells with thinner electrodes, due to the higher volumetric/resistance ratio of the separator within the cell. However, our findings revealed the opposite case: in the cells with thick electrodes, substantial differences in DC-IR and capacity retention at high rates were observed based on the type of separator used. In contrast, such differences were negligible in thin electrode configurations. As confirmed by the simulation results, the higher current density in thicker electrode cells leads to an ion concentration difference in the upper region of the electrodes, depending on separator resistance. Additionally, the increased thickness and R_{ion} of the electrodes can hinder Li^+ transfer from the upper to the lower regions. These results demonstrate that the intrinsic properties of individual cell components, such as separator porosity, may not always manifest, but rather depend on the overall cell design. This underscores the importance of considering the interplay between electrode design and separator characteristics when optimizing LIB performance. Furthermore, carefully selecting separators for high-safety LIBs, considering both thermal stability and mechanical strength, is very crucial. Consequently, this study highlights the combined effect between electrode design and separator porosity in LIBs and underscores the importance of balancing safety and power performance in cell design.

Experimental Section

Electrode Preparation

The cathode slurry was prepared by mixing 93 wt% NCM622 (L&F, Korea) as the active material, 4 wt% conductive agent (Super P Li®),

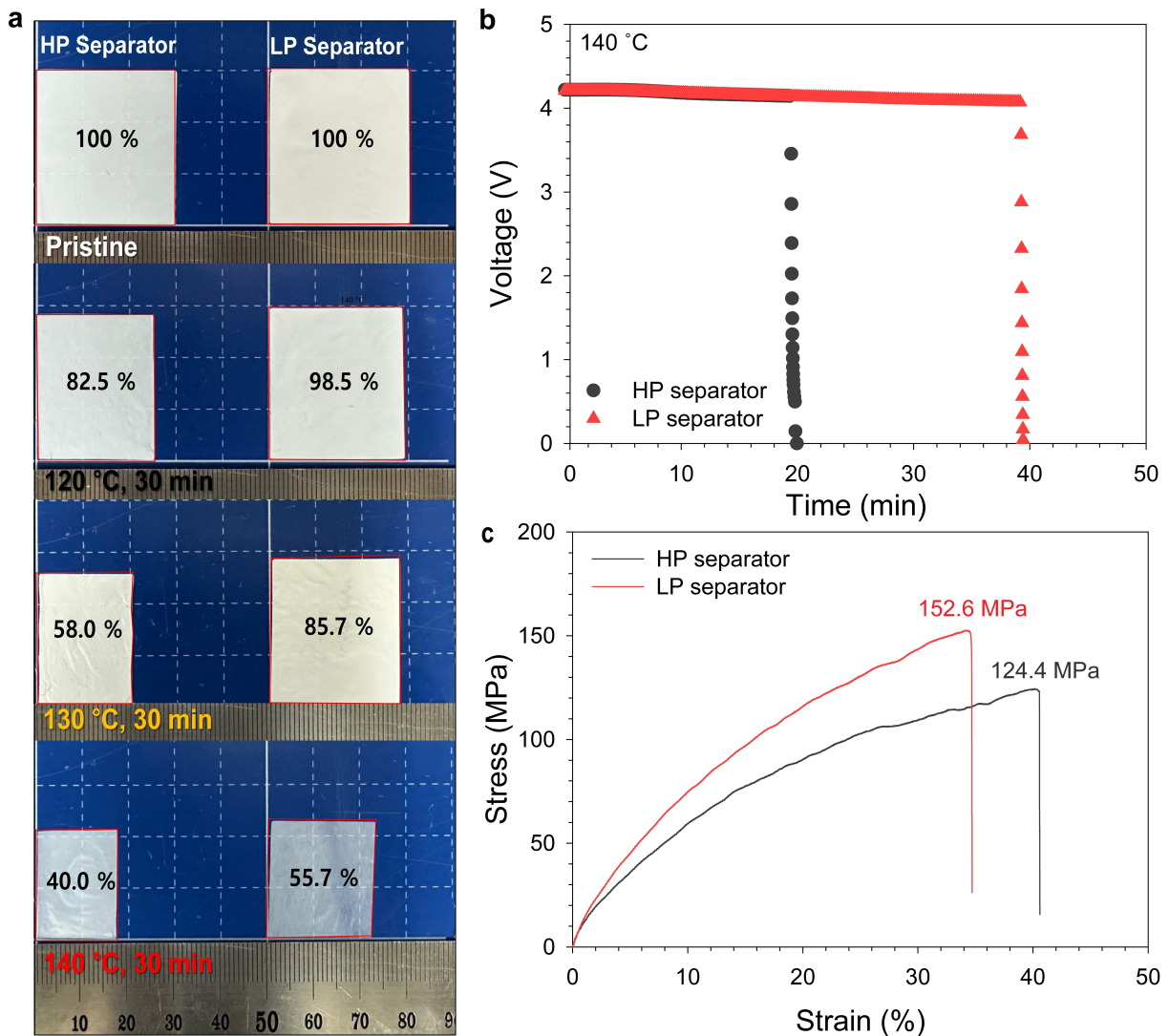


Figure 5. (a) Digital camera images of the high porosity (HP) and low porosity (LP) PE separators after exposure to high temperatures (120, 130, and 140 °C for 30 min, sample size = 3 cm×3 cm). (b) comparison of the OCV change of pouch cells assembled with the HP and LP separators during exposure to 140 °C. (c) stress-strain curves of the HP and LP separators in machine direction.

Imerys Graphite & Carbon, Switzerland), and 3 wt% polyvinylidene fluoride (PVdF; KF-1300, M_w = 350,000, Kureha, Japan) as a binder. The prepared slurry was uniformly coated onto an aluminum foil (15 µm, Sam-A Aluminum, Korea) with different loading levels by controlling the doctor-blade gap. The coated slurry was then dried in an oven at 130 °C for 1 h, followed by pressing with a gap-control-type roll-pressing machine (CLP-2025, CIS, Korea). Similarly, the anode slurry was also prepared by mixing 96.9 wt% artificial graphite (SCMG-AR, Showa Denko, Japan) as the active material, 0.5 wt% conductive agent, and 2.6 wt% styrene-butadiene rubber (SBR; Zeon Corporation, Japan)/carboxymethyl cellulose (CMC; Dai-Ichi Kogyo Seiyaku, Japan) as a binder. The as-prepared slurry was coated onto a copper foil (10 µm, LOTTE Energy Materials, Korea) with different loading levels by controlling the doctor-blade gap. After coating, the slurry was dried in an oven at 60 °C for 2 h and subsequently pressed using a gap-control-type roll-pressing machine. Detailed design parameters for both the cathode and anode are provided in Table 2.

Table 2. Design parameters of the electrodes.

Design parameter	Unit	Cathode	Anode
Composition	wt %	93 (NCM622) 4 (Super P) 3 (PVdF)	96.9 (Graphite) 0.5 (Super P) 1.3/1.3 (SBR/CMC)
Loading level (Thin/Thick)	mg cm ⁻²	9.4/23.5	4.9/12.3
Electrode Density	g cm ⁻³	3.0	1.56
Electrode thickness (Thin/Thick)	µm	31/78	31/79
Current collector thickness	µm	15 (Al)	10 (Cu)

Electrical Resistance Measurement

To characterize an ionic resistance (R_{ion}) of cathodes and anodes, symmetric cell EIS was measured in NCM622 || separator || NCM622 and graphite || separator || graphite symmetric cells. The cells were assembled using a 1.15 M solution of LiPF₆ dissolved in a mixture of ethylene carbonate (EC) and ethyl methyl carbonate (EMC) (3:7, v/v, Enchem, Korea) as the electrolyte. Measurements were conducted using an electrochemical analysis system (VSP-300 Potentiostat, BioLogic, France) over a frequency range from 5 MHz to 200 mHz, with an AC amplitude of 10 mV. Utilizing equivalent circuit model (Figure S10),^[43] the ionic resistance was determined from EIS data.

Both bulk and electrode/current collector interfacial resistances of cathodes and anodes were measured using an electrode resistance measuring instrument (RM2610, Hioki, Japan). The operating current and voltage ranges were 0–1 mA and 0–0.5 V, respectively.

Characterization of the Separator

The surface morphology of the separators was examined via field-emission scanning electron microscopy (FE-SEM, S-4800, Hitachi, Japan). Deionized (DI) water contact angles were measured using a drop shape analyzer (DSA 100, KRUSS, Germany), while air permeability was evaluated using a densometer (4110 N, Thwing-Albert, USA). The air permeability measurements involved measuring the time taken for 100 mL of air to pass through 1 in.² of the separator under a pressure differential of 0.176 psi. To evaluate the ionic conductivity (σ) of the separators, 2032-type coin cells comprising SUS/separator/SUS were assembled. The bulk resistance (R_b) was measured using an electrochemical analysis system (VSP-300 Potentiostat, BioLogic, France) across a frequency range of 1 MHz to 50 kHz at an amplitude of 10 mV. The ionic conductivity (σ) was then calculated using the following equation:

$$\sigma = I / (R_b \cdot S)$$

where I is the thickness of the separator, and S is the area of the SUS electrode. Thermal shrinkage of the separator was measured before and after storage in a convection oven at 120, 130, and 140°C for 30 min to assess its thermal stability at high temperatures. The thermal shrinkage was acquired by the following equation:

$$\text{Thermal shrinkage}[\%] = \left(\frac{A_{\text{before}} - A_{\text{after}}}{A_{\text{before}}} \right) \times 100$$

where A_{before} and A_{after} refer to the area of the separators before and after storage in the convection oven, respectively. The mechanical properties of the separators were analyzed using a universal testing machine (UTM, United Calibration, USA).

Cell Assembly

2032-type coin cells were assembled with an NCM622 || Graphite configuration in a controlled environment within a glove box with a dew point below –80°C. The NCM622 cathode and artificial graphite anode were punched into 14 mm and 16.2 mm discs, respectively. Two types of PE separators (W-Scope Korea, Korea) with different porosities were used (diameter = 18 mm, thickness = 9 µm). Prior to cell assembly, all electrodes and separators underwent a 12-hour drying process at 60°C in a vacuum oven. The liquid electrolyte was prepared by dissolving 1.15 M LiPF₆ in a mixture of EC and EMC (3/7, v/v, Enchem, Korea).

Electrochemical Analysis

The fabricated 2032-type coin cells were aged for 12 h to ensure adequate wetting of the electrodes and separator with the liquid electrolyte. Subsequently, the cells underwent pre-cycling within a voltage range of 3.0–4.3 V. It includes initial charging and discharging at a constant current (CC) of 0.1 C-rate as a formation step and further charging in constant current/constant voltage (CC/CV) mode and discharging in CC mode at a rate of 0.2 C for additional three cycles as a stabilization step. After pre-cycling, the DC-IR was measured using a HPPC protocol. This involved a 5 C-rate discharge for 10 s, followed by 40 s rest time, and then a 3.75 C-rate charge for 10 s. DC-IRs were measured repeatedly at every 20% interval between SOC of 20% and 100%. The rate capability of the cells was assessed by varying the discharge C-rate, ranging from 0.5 C to 10 C (0.5 C, 1 C, 2 C, 3 C, 5 C, 7 C, 10 C, and 0.5 C) while maintaining a constant charging C-rate of 0.5 C in CC/CV mode between 3.0 and 4.3 V. The cycle performance at 0.5 C and 3 C-rate was also evaluated at 25°C between 3.0 and 4.3 V for 100 cycles (CC/CV mode in charging and CC mode in discharging).

Computational Analysis

An electrochemical model was developed using COMSOL Multiphysics 6.2 (COMSOL Inc., USA) to analyze the effect of the separator on the power performance of various types of electrodes. Based on the model proposed by Doyle and Newman,^[47] we built an electrochemical model in a pseudo-3-dimensional space comprising x, y, and pseudo-r dimensions.^[48] Particularly, in this model, the tortuosity of the separator was back-calculated based on the experimentally obtained electrochemical properties of the actual separator, and the diffusion/migration behavior of lithium ions within the separator was simulated using the tortuosity and known porosity data (Table S1). The geometry of the electrode reflected the actual electrode dimensions, as summarized in Table 1, and further details on the model geometry, parameters, and governing equations are provided in the supporting information (Figure S11 and Table S2–S4).

Acknowledgements

This research was supported by the Industrial Technology Innovation Program (RS-2022-00155854) funded by the Korean Ministry of Trade, Industry, and Energy (MOTIE). The authors are also grateful for the support from the DGIST Supercomputing and Big Data Center.

Conflict of Interests

The authors declare no conflict of interest.

Data Availability Statement

The data that support the findings of this study are available from the corresponding author upon reasonable request.

Keywords: Lithium-ion battery • Porosity • Power • Separator • Thick electrode

- [1] J.-M. Tarascon, M. Armand, *Nature* **2001**, *414*, 359–367.
- [2] M. M. Thackeray, C. Wolverton, E. D. Isaacs, *Energy Environ. Sci.* **2012**, *5*, 7854–7863.
- [3] M. Li, J. Lu, Z. Chen, K. Amine, *Adv. Mater.* **2018**, *30*, 1800561.
- [4] M. R. Showalter, J. J. Lissauer, *Science* **2006**, *311*, 973–977.
- [5] S. S. Zhang, *J. Power Sources* **2006**, *162*, 1379–1394.
- [6] T. Ohzuku, R. J. Brodd, *J. Power Sources* **2007**, *174*, 449–456.
- [7] A. Mishra, A. Mehta, S. Basu, S. J. Malode, N. P. Shetti, S. S. Shukla, M. N. Nadagouda, T. M. Aminabhavi, *Mater. Sci. Energy Technol.* **2018**, *1*, 182–187.
- [8] R. Mukherjee, R. Krishnan, T. M. Lu, N. Koratkar, *Nano Energy* **2012**, *1*, 518–533.
- [9] D. Zhang, C. Tan, T. Ou, S. Zhang, L. Li, X. Ji, *Energy Rep.* **2022**, *8*, 4525–4534.
- [10] K. X. Wang, X. H. Li, J. S. Chen, *Adv. Mater.* **2015**, *27*, 527–545.
- [11] K. Deng, Q. Zeng, D. Wang, Z. Liu, G. Wang, Z. Qiu, Y. Zhang, M. Xiao, Y. Meng, *Energy Storage Mater.* **2020**, *32*, 425–447.
- [12] D. Hubble, D. E. Brown, Y. Zhao, C. Fang, J. Lau, B. D. McCloskey, G. Liu, *Energy Environ. Sci.* **2022**, *15*, 550–578.
- [13] Q. Wang, L. Jiang, Y. Yu, J. Sun, *Nano Energy* **2019**, *55*, 93–114.
- [14] M. Singh, J. Kaiser, H. Hahn, *J. Electrochem. Soc.* **2015**, *162*, A1196–A1201.
- [15] H. Zheng, J. Li, X. Song, G. Liu, V. S. Battaglia, *Electrochim. Acta* **2012**, *71*, 258–265.
- [16] J. Jeong, H. Lee, J. Choi, M. H. Ryou, Y. Min Lee, *Electrochim. Acta* **2015**, *154*, 149–156.
- [17] Y. Liu, M. Clark, Q. Zhang, D. Yu, D. Liu, J. Liu, G. Cao, *Adv. Energy Mater.* **2011**, *1*, 194–202.
- [18] J. Choi, B. Son, M.-H. Ryou, S. H. Kim, J. M. Ko, Y. M. Lee, *J. Electrochem. Sci. Technol.* **2013**, *4*, 27–33.
- [19] Y. Kuang, C. Chen, D. Kirsch, L. Hu, *Adv. Energy Mater.* **2019**, *9*, 1901457.
- [20] J. Park, C. Jeon, W. Kim, S. J. Bong, S. Jeong, H. J. Kim, *J. Power Sources* **2021**, *482*, 228948.
- [21] R. Zhao, J. Liu, J. Gu, *Appl. Energy* **2015**, *139*, 220–229.
- [22] J. A. Choi, S. H. Kim, D. W. Kim, *J. Power Sources* **2010**, *195*, 6192–6196.
- [23] G. Venugopal, J. Moore, J. Howard, S. Pendalwar, *J. Power Sources* **1999**, *77*, 34–41.
- [24] D. V. Horváth, R. Tian, C. Gabbett, V. Nicolosi, J. N. Coleman, *J. Electrochem. Soc.* **2022**, *169*, 030503.
- [25] H. Lee, M. Yanilmaz, O. Toprakci, K. Fu, X. Zhang, *Energy Environ. Sci.* **2014**, *7*, 3857–3886.
- [26] X. Huang, *J. Solid State Electrochem.* **2011**, *15*, 649–662.
- [27] Y. Roh, D. Jin, E. Kim, S. Byun, Y. S. Lee, M. H. Ryou, Y. M. Lee, *Chem. Eng. J.* **2022**, *433*, 134501.
- [28] Z. Liu, Y. Jiang, Q. Hu, S. Guo, L. Yu, Q. Li, Q. Liu, X. Hu, *Energy Environ. Mater.* **2021**, *4*, 336–362.
- [29] M. F. Lagadec, R. Zahn, V. Wood, *Nat. Energy* **2019**, *4*, 16–25.
- [30] C. M. Costa, Y. H. Lee, J. H. Kim, S. Y. Lee, S. Lanceros-Méndez, *Energy Storage Mater.* **2019**, *22*, 346–375.
- [31] S. Choi, U. Kim, Y. Roh, C. B. Dzakpasu, J. Lim, M. Song, J. Rhee, Y. S. Lee, Y. M. Lee, *J. Power Sources* **2024**, *623*, 235427.
- [32] U. Kim, Y. Roh, S. Choi, Y. S. Lee, S. Y. Ryou, Y. M. Lee, *J. Ind. Eng. Chem.* **2023**, *126*, 137–144.
- [33] D. V. Horváth, R. Tian, C. Gabbett, V. Nicolosi, J. N. Coleman, *J. Electrochem. Soc.* **2022**, *169*, 030503.
- [34] D. Djian, F. Alloin, S. Martinet, H. Lignier, J. Y. Sanchez, *J. Power Sources* **2007**, *172*, 416–421.
- [35] R. E. Sousa, J. Nunes-Pereira, C. M. Costa, M. M. Silva, S. Lanceros-Méndez, J. Hassoun, B. Scrosati, G. B. Appetecchi, *J. Power Sources* **2014**, *263*, 29–36.
- [36] Y. Lee, J. Park, H. Jeon, D. Yeon, B. H. Kim, K. Y. Cho, M. H. Ryou, Y. M. Lee, *J. Power Sources* **2016**, *325*, 732–738.
- [37] W. U. Arifeen, M. Kim, J. Choi, K. Yoo, R. Kurniawan, T. J. Ko, *Mater. Chem. Phys.* **2019**, *229*, 310–318.
- [38] W. Miao, J. Wang, G. Li, S. Liu, X. Luo, *J. Energy Storage* **2023**, *66*, 107353.
- [39] X. Leng, M. Yang, C. Li, W. U. Arifeen, T. J. Ko, *Chem. Eng. J.* **2022**, *433*, 133773.
- [40] N. Ogihara, S. Kawauchi, C. Okuda, Y. Itou, Y. Takeuchi, Y. Ukyo, *J. Electrochem. Soc.* **2012**, *159*, A1034–A1039.
- [41] N. Ogihara, Y. Itou, T. Sasaki, Y. Takeuchi, *J. Phys. Chem. C* **2015**, *119*, 4612–4619.
- [42] J. Landesfeind, J. Hattendorff, A. Ehrl, W. A. Wall, H. A. Gasteiger, *J. Electrochem. Soc.* **2016**, *163*, A1373–A1387.
- [43] H. Nara, D. Mukoyama, R. Shimizu, T. Momma, T. Osaka, *J. Power Sources* **2019**, *409*, 139–147.
- [44] N. Y. Kim, J. Moon, M. H. Ryou, S. H. Kim, J. H. Kim, J. M. Kim, J. Bang, S. Y. Lee, *Adv. Energy Mater.* **2022**, *12*, 2102109.
- [45] K. Kim, S. Byun, J. Choi, S. Hong, M. H. Ryou, Y. M. Lee, *ChemPhysChem* **2018**, *19*, 1627–1634.
- [46] Y. Son, H. Cha, T. Lee, Y. Kim, A. Boies, J. Cho, M. De Volder, *Energy Environ. Mater.* **2023**, *7*, e12615.
- [47] M. Doyle, J. Newman, A. S. Gozdz, C. N. Schmutz, J.-M. Tarascon, *J. Electrochem. Soc.* **1996**, *143*, 1890.
- [48] J. Kang, J. Lim, H. Lee, S. Park, C. Bak, Y. Shin, H. An, M. Lee, M. Lee, S. Lee, B. Choi, D. Kang, S. Chae, Y. M. Lee, H. Lee, *Adv. Sci.* **2024**, *11*, 2403071.

Manuscript received: September 30, 2024

Revised manuscript received: December 22, 2024

Accepted manuscript online: December 24, 2024

Version of record online: January 8, 2025